ACS OMEGA

http://pubs.acs.org/journal/acsodf

Article

Secondary Flow Effect on Supercritical Kerosene Oxidation Deposition and Heat Transfer in a Coiled Tube

Xinyan Pei,* Hongyu Tian, Zekun Zheng, Yafen Wang, and Lingyun Hou*

Cite This: *ACS Omega* 2022, 7, 23978−23987

Read Online

ACCESS | Metrics & More | Article Recommendations

ABSTRACT: Deposition in fuel cooling systems remains a challenge to the development of active cooling technologies for air-breathing engines. We experimentally and numerically investigated the influence of the secondary flow and heat-transfer characteristics of supercritical kerosene in a coiled tube on oxidation deposition. A coiled heated tube reactor (3000 mm long, 23 cycles) under constant heat flux and flow rate was applied to simulate the conditions of the fuel side in the heat exchanger of an aero-engine cooling system. The coupling characteristics of coking distribution with the development of secondary flow were studied along the whole pipe. The dynamic pressure, temperature, and velocity were analyzed in two specific circular cross sections located in the bend of the tube. The secondary flows induced in the coiled tube greatly enhance the heat transfer and slightly decrease the deposition rate, resulting in linear wall temperature profiles and a uniform coking distribution along the tube compared to the long straight tube. There is no obvious heat-transfer enhancement or deterioration in the whole coiled tube. The modified heat-transfer correlation of the supercritical RP-3 in the coiled tube was fitted at different flow rates and heat fluxes with an error of ±10%.

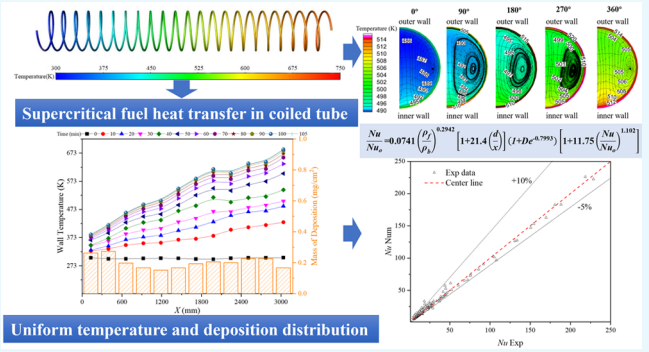

1. INTRODUCTION

With the development of aero-engine technology, the increased thrust of the engine requires a higher supercharging ratio and turbine inlet temperature. The increase of the pressure ratio leads to a higher compressor outlet temperature of the air, part of which is applied to cool the turbine fan. In addition, in the combustor, the temperature of the outlet increases significantly as a result of high-temperature combustion, which increases the heat load of the turbine. In the next-generation engine, the maximum operating temperature of the turbine will reach 2400 K. To ensure the operative condition of the turbine at high temperature, researchers have proposed the CCA (cooled cooling air) cooling technology of adding a heat exchanger on the aero-engine. In 1999, Bruening et al.[1] designed a way to improve the quality of cooling gas by using this heat-exchange method on military aircraft. To enhance the performance of the cooling air, a heat exchanger is installed on the bypass of the aero-engine, and the aviation fuel is used as the heat sink to precool the air used for the cooling of the turbine.

Using aviation fuel as the cooling medium can reduce the temperature of the air used for cooling and also improve the cooling efficiency of high-temperature components. At the same time, using aviation fuel as a cooling medium instead of using the air of engine bypass will not cause adverse problems such as pressure loss of bypass. In addition, there are some other advantages. When the fuel temperature increases, the fuel will be in a supercritical state. In this state, the physical properties of the fuel will change significantly. For example, the density of the fuel will decrease, the surface tension will disappear, and the diffusion ability will be enhanced. Therefore, the atomization effect and the combustion efficiency will be substantially improved. Because of the physical characteristics of aviation kerosene, the air−fuel heat exchanger is a possible way to reduce the temperature of cooling air for advanced aero-engines.

There has been much research on air−fuel heat exchangers. Tibbs[2] explored a way to extend the service life of an air-fuel heat exchanger. Nir[3] designed a heat exchanger with three kinds of fluid flows. The first and second series of tube bundles were used to circulate the first and second fluid, respectively. The third fluid was circulated between the two tube bundles and the shell, which contacts the two tube bundles and exchanges heat with the first two fluids and finally realizes heat

Received: May 8, 2022
Accepted: June 16, 2022
Published: June 28, 2022

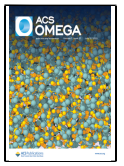

https://doi.org/10.1021/acsomega.2c02848
ACS Omega 2022, 7, 23978−23987

exchange among the three fluids. Nacke[4] designed an air−fuel heat exchanger model suited for the high Mach number. The heat exchanger adopts a method of differential heat-transfer rate calculation and integration to achieve a highly modular design with small size and lightweight. Nacke et al.[5] proposed another compact and efficient high-Mach-number air-fuel heat exchanger, consisting of closely arranged modules composed of microchannels and fins. Holmes et al.[6] designed a compact compressor heat exchanger for natural gas. By comparing the structural parameters of various heat exchangers, they finally chose a compact heat exchanger and used a panel design with heat pipes. Manteufel et al.[7] arranged a heat exchanger with a rectangular microchannel structure as the liquid kerosene flow channel. Kim et al.[8] studied the heat-transfer and flow characteristics of an air−fuel heat exchanger with high-speed external duct flow and observed the cooling effect by adopting different installation positions and methods. Sundén et al.[9] expounded the influence of fin change on the heat exchange area and calculated the influence of several fin types on the change in temperature and pressure of the heat exchanger through data by changing the shape and fins arrangement. Based on the research prospect of using an air-fuel heat exchanger in aero-engines, it is necessary to adopt an efficient and compact heat-transfer mode and structure. Although the heat-transfer performance of aviation fuel is better than that of air, fuel chemical reactions such as the oxidation coking reaction will occur at high temperature so that the life of the heat exchanger is reduced.

When the aviation fuel acts as the coolant in the engine cooling system, it reacts with dissolved oxygen and oxygenated compounds at temperatures ranging from 423 to 723 K to form coke deposition on the inner surface of the fuel channel of the heat exchanger, which can deteriorate the heat transfer and even block fuel flow.[10] The autoxidation chain can be terminated by reducing the concentration of dissolved oxygen.[11] Temperature is also a critical factor in determining the thermal oxidation reaction process of fuel.[12] When the fuel temperature rises above 421 K, the dissolved oxygen begins reacting with the components in the fuel to generate coking precursors and then initiates a series of free-radical chain reactions to generate coking. This form of coking is mainly caused by thermal-oxidative reactions, so it is called thermal oxidation coking. When the fuel temperature is lower than 644 K, the dissolved oxygen in the fuel is the main influencing factor for coking. In this temperature range, the concentration of dissolved oxygen dramatically affects the formation rate of coking. With a temperature increase, the rate of the thermal oxidation reaction accelerates and reaches a peak at 644 K. After the consumption of dissolved oxygen, the thermal oxidation reaction gradually ends. As the fuel temperature continues to rise to approximately 700 K, the coking reaction mechanism begins to change to the stage of the thermal cracking reaction. In the pyrolysis reaction, the chemical bonds are broken into smaller alkanes and some hydrogen elements, forming coking deposits. This form of coking is called pyrolysis coking.[13,14]

Coking will cause the cooling pathway to be blocked, reducing mechanical properties, and coking products will block the nozzle of the engine, affecting the performance of the engine.[15] Thus, thermal stability and heat-transfer characteristic studies are very important for the application of active fuel cooling technology. Temperature is the main factor affecting the coking of aviation kerosene; in addition, pressure and surface materials are also important factors affecting coking. Watt et al.[16] found that within the pressure range of 0.017−4.24 MPa both the total amount of coking and the local amount of coking decreased with pressure, indicating that the increase in pressure could inhibit the fuel coking. Jones et al.[17] studied the influence of surface materials on coking and verified the catalytic effect of metal surfaces on oxidative coking. But surface passivation treatment can reduce the coking rate. The structure of a heat exchanger pipe is also an important factor affecting coking. Previous studies on the oxidation deposition properties of liquid fuel were mainly conducted in straight tubes.[18−21] The geometry of the tube defines the flow regime, which has a significant impact on the deposition process and heat-transfer characteristics. The helically coiled tube is widely used as a heat exchanger in various cooling systems. Yildiz et al.[22] analyzed the pressure drops and heat transfer of helical tubes at different air inlet flow rates. The higher heat-transfer rate and pressure drop in the helical pipe are due to the secondary flow of the fluid. An increase in momentum transfer results in the growth in the rate of heat transfer. Rao et al.[23] measured the fully developed turbulent fanning friction factors and Nusselt numbers for purely viscous power-law non-Newtonian fluids in helical coils through experiments and a new equation of the turbulent friction coefficient was proposed. Austen et al.[24] explored the influence of pitch on the pressure drop and heat-transfer characteristics of helical coils under the uniform input heat flux. In their study, the pitch affects the friction factor and the Nusselt number. Chingulpitak et al.[25] tested the effects of various geometries of helical capillary tubes on the flow characteristics of alternative refrigerants and demonstrated that the length of helical capillary tubes was affected by coil diameter variation (less than 300 mm) for helical capillary tube geometries. Ferng et al.[26] gave a computational fluid dynamics methodology to investigate the effects of different pitch sizes and Dean numbers on the thermal-hydraulic characteristics of a helically coil-tube heat exchanger. In their study, the CFD methodology can capture the thermal and hydraulic characteristics such as flow acceleration and separation in the shell side, secondary flow on the tube side etc. Zhang et al.[27] experimentally studied the heat-transfer characteristics of supercritical CO_2 by heating it in a vertical helical tube with an inner diameter of 9 mm and developed correlations for the heat-transfer coefficient. Wang et al.[28] carried out a numerical simulation of the heat-transfer performance of heated supercritical CO_2 in a helical tube and found that the secondary flow pattern caused by buoyancy was similar to that caused by centrifugal force. Centrifugal force causes the fluid to flow faster on the outside of the helical tube than inside the tube. Ebadian et al.[29,30] used numerical methods to study the effects of different bending diameters and pitches on a specific fluid flow in a spiral tube under the constant heat flux and wall temperature conditions. It was found that the temperature distribution of the circular cross-section was asymmetric with the increasing pitch in laminar flow.

In summary, many researchers only focused on the heat-transfer investigation of supercritical fluids such as water and CO_2.[27,31,32] In contrast, research on the deposition process and heat-transfer characteristics of supercritical kerosene, especially in the structure of helically coiled tubes in heat exchanger applications, is still lacking. The present study carried out experimental work and numerical simulation on the heat transfer and oxidation deposition of aviation kerosene RP-3

https://doi.org/10.1021/acsomega.2c02848
ACS Omega 2022, 7, 23978−23987

under a supercritical pressure in the helically coiled tube. The influence of secondary flow on oxidation deposition from heated kerosene is revealed. In addition, we analyzed the deposition and heat transfer of a single coil of the helically coiled tube.

2. EXPERIMENTAL AND NUMERICAL METHOD

2.1. Experimental setup. Standard Chinese aviation kerosene (RP-3) was chosen as the coolant fuel. The critical temperature and pressure of RP-3 are 645.5 K and 2.39 MPa, respectively.[33] The density and relative molecular weight of kerosene at room temperature are 0.7913 g/cm^3 and 148.33 g/mol, respectively. Details of the experimental setup and measurement systems are provided in Figure 1. The amount

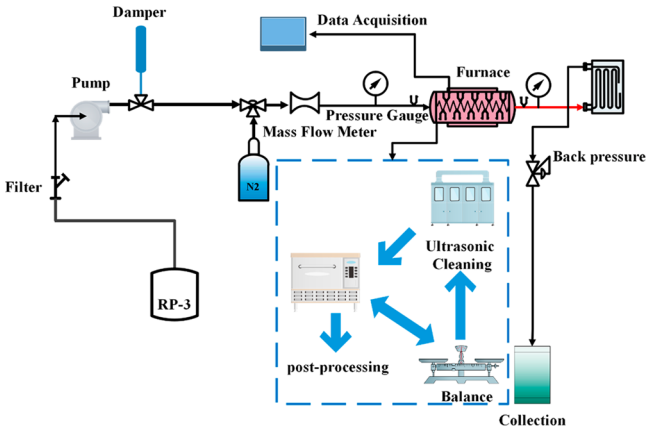

Figure 1. Schematic of the experimental setup.

of deposition was evaluated by the weighing method, which has been successfully applied and verified in our previous research.[34] The shapes of the fuel cooling path have a significant influence on the heat transfer and deposition process, in which one of the widely used cooling structures is the coiled tube pathway due to its compact feature. Therefore, a coiled heated tube reactor under the constant heat flux and the flow rate was applied to simulate the heat-exchanger in an aero-engine cooling system. The structure, thermocouple measurement position, parameters, and characteristics of the coiled are provided in Figure 2a,b. The helically coiled tube, as a form of 3000 mm long and 23 cycles, is made of 316 stainless steel with an inner diameter of 2 mm and a wall thickness of 0.5 mm. In Figure 2b, a coil pitch, P, and a coil radius, R, are 22 and 50 mm, respectively.

In the experiment, the heating time was set to 1.75 h to ensure thermal balance for the flow. The mass flow rate is 1 g/s, and the temperature at the entrance is set at 300 K with a constant heat flux of 60 kW/m^2 under the pressure condition of 3 MPa. The heat-transfer coefficient of the experiment can be calculated as follows

$$h = q/(T_w - T_b) \tag{1}$$

where q is the heat flux, which depends on the heating power and excludes the heat loss, T_w is the temperature of the wall, and T_b is the temperature of the kerosene. The uncertainty of heat flux results from the heating voltage and current. The local temperature difference consists of the deviation between the outer wall and the fuel temperature. The uncertainty of the local convective heat-transfer coefficient is composed of heat flux, local temperature difference, and experimental instrument error. Moreover, the uncertainty of the mass flow rate is ±0.2, and the uncertainty of the pressure is ±1%.

$$\text{uncertainty of heat flux: } \left|\frac{\partial Q_1}{Q_1}\right| = \sqrt{\left(\frac{\partial I}{I}\right)^2 + \left(\frac{\partial I}{I}\right)^2} = 5.055\% \tag{2}$$

$$\text{uncertainty of heat flux: } \left|\frac{\delta(\Delta T)}{\Delta T}\right| \le \frac{\sqrt{(\delta T_w)^2 + (\delta T_F)^2}}{\Delta T_{max}} \approx 7.1\% \tag{3}$$

$$\text{heat-transfer coefficient: } \left(\frac{\delta h_x}{h_x}\right) = \sqrt{\left(\frac{\delta Q}{Q}\right)^2 + \left(\frac{\delta F}{F}\right)^2 + \left(\frac{\delta(\Delta T)}{\Delta T}\right)^2} \le 10\ \% \tag{4}$$

2.2. Numerical Model. A commercial software, Ansys Fluent,[35] was utilized to solve the steady and three-dimensional flow as well as heat transfer in the coiled tube model. The turbulent model of standard $k - \varepsilon$ was applied by considering the transition from laminar flow to turbulent flow, which has been verified and widely used in the relevant investigation on the coiled tube.[26,29] The governing equations in finite volume form were solved iteratively by using a second-order upwind scheme. In addition, the SIMPLEC pressure–velocity coupling scheme was employed in the solution of the momentum equations. When the normalized error residuals for all of the calculated variables are reduced to 6 orders of magnitude below their maxima, the solution is deemed to be converged. The boundary conditions of the simulation are coincidental to the experiment. The mesh of the cross-section of the coiled tube is the o-grid, and the independent study on mesh has been conducted. After the grid independence study, the total number of mesh cells used in the numerical simulation is optimized as 596,160. The thermal physical properties of the aviation kerosene are temperature-dependent and defined by using a three-component surrogate model in our previous simulation.[33,36] When the flow state is close to the critical point, small changes in pressure or temperature result in significant changes in the thermal properties and the fuel becomes a supercritical fluid with gaslike diffusivity, density,

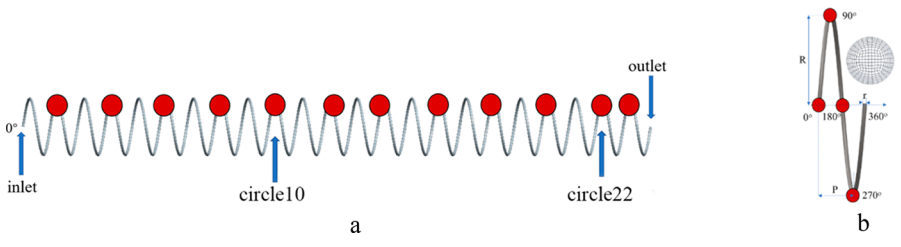

Figure 2. Structure and parameters of the coiled and thermocouple locations (a, structure; b, parameters).

https://doi.org/10.1021/acsomega.2c02848
ACS Omega 2022, 7, 23978−23987

and viscosity.[21] The specific heat capacity increases sharply near the critical temperature, the density decreases sharply, and the thermal conductivity reaches a low value. The deposition process and the chemical reactions of thermal oxidation coking were neglected in the simulation.

3. RESULTS AND DISCUSSION

The experimental wall temperature and deposition profiles along the tube as the increase of heating time are shown in Figure 3. The fuel temperature and the local wall temperature

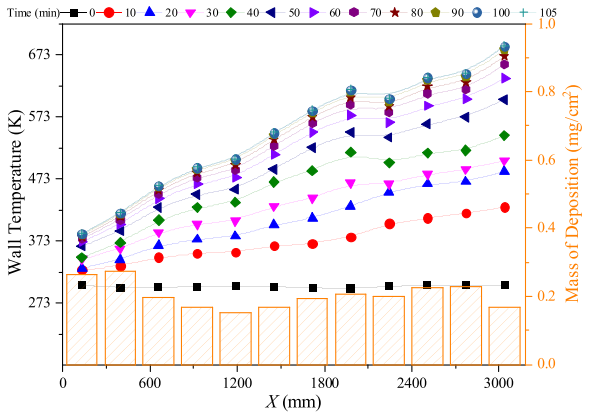

Figure 3. Measured wall temperature and deposition profiles along the tube.

are linearly increased along the tube. The slope of the wall temperature profile is increased as the heating proceeds. There is a slight fluctuation in the mass distribution of deposition along the tube. In our previous study,[11] we conducted the deposition experiment in a straight tube reactor with the same heating time, flow rate, and outlet fuel temperature compared to the coiled tube experiment. In comparison with the situation of the coiled tube in Figure 3, the wall temperature distribution along the straight tube has many fluctuations, and its values are nearly 100 K higher than that of the coiled tube because secondary flows in the coiled tube enhance the heat transfer of the flow. In addition, the inlet effect is not very obvious on the deposition near the inlet because of the entrainment effect of the secondary flow on the boundary layer in the coiled tube compared to the straight tube. The average deposition rate of the coiled tube is 0.1162 mg/cm^2.h, which is higher than that of 0.1036 mg/cm^2·h in the straight tube.[33] Under the turbulent conditions of the relatively high Re number, the heat and mass exchanges are enhanced and there is a thinner boundary layer, which benefits the deposition process.[33] To illustrate the secondary flow effect on the coiled tube, we compared the deposition result of the coiled tube to that in straight tubes under similar experimental conditions. Zhu et al.[37] conducted an oxidation coking experiment on supercritical aviation kerosene for 1 h in a 1.6 m long straight pipe with an external diameter of 2.2 mm and internal diameter of 1.78 mm, setting the inlet temperature at 403 K and the outlet temperature at 723 K. There was a unimodal deposition rate up to 0.8 mg/cm^2/h in the middle of the test section in this experiment, and the deposition rate was around 0.1 mg/cm^2·h in the other section. Liu et al.[38] improved a kinetic model for deposition through thermal oxidation of aviation hydrocarbon fuels experiment. Their reactive tube was 1.9 m long with 2.2 mm outside diameter and 1.8 mm inside diameter. The experiment lasted for 3 h, and the fuel flow rate was 1 g/s. The inlet temperature was 300 K, and the outlet temperature was 710 K. The average deposition rate in their experiment was about 0.1 mg/cm^2·h. The coke distribution in the tube was not uniform; there are deterioration areas with much more coking, which would cause partial blockage of the straight pipe. The coiled tube makes the coke distribution more uniform because there is no local bonding deterioration of the secondary flow.

Figure 4 shows the fuel temperature and Reynolds number along the coiled tube. The Reynolds number increases rapidly

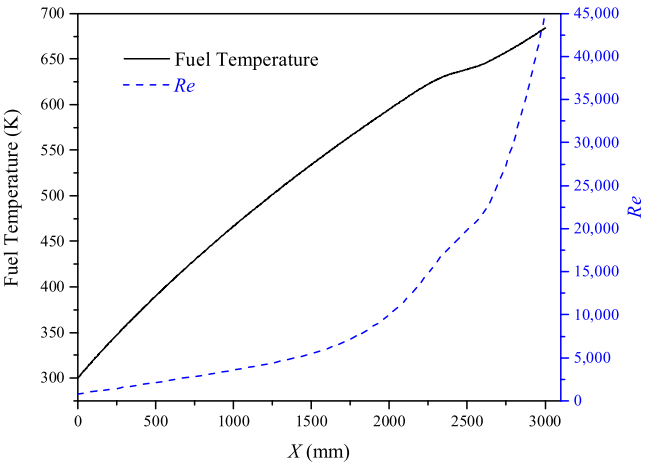

Figure 4. Fuel temperature and Reynolds number along the coiled tube.

in the back part of the tube because the temperature at the back part of the tube is close to the supercritical temperature of fuel and the density and viscosity change significantly, which leads to the Reynolds number rising sharply. As shown in Figure 5, some deviations occur at the first 1000 mm of the tube between experimental data and numerical simulation results due to the inlet effect in actual flow. In the front section of the flow pipeline, the experimental value is generally higher than the numerical simulation result, while in the back section of the flow pipeline, the two results approach. Experimental

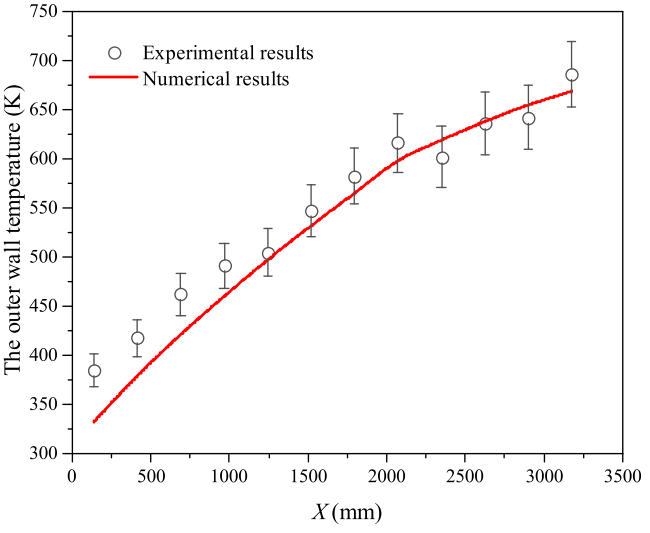

Figure 5. Comparison of outer wall temperature between experimental and numerical results.

https://doi.org/10.1021/acsomega.2c02848
ACS Omega 2022, 7, 23978−23987

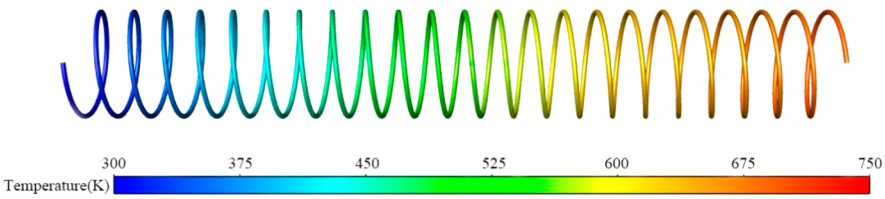

Figure 6. Outer wall temperature contour.

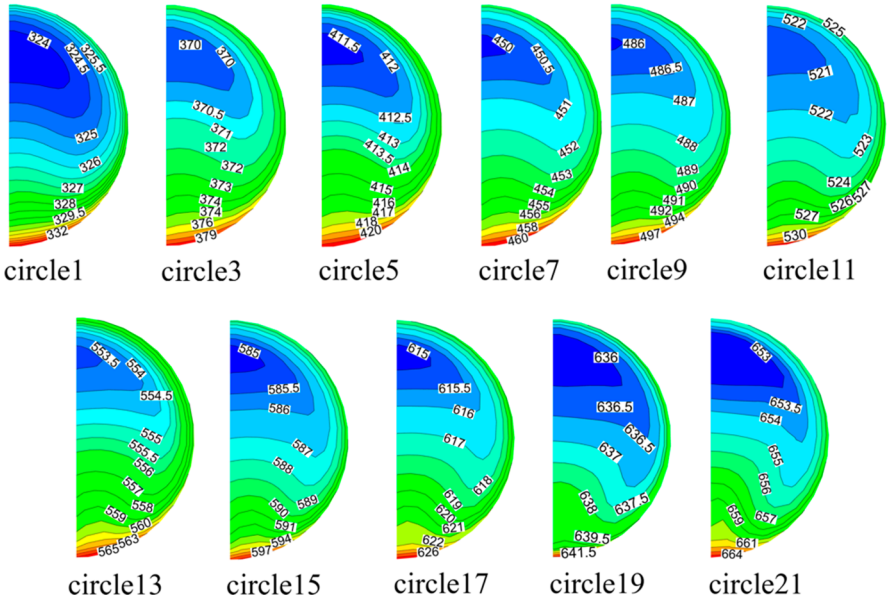

Figure 7. Cross-section temperature along the coiled tube.

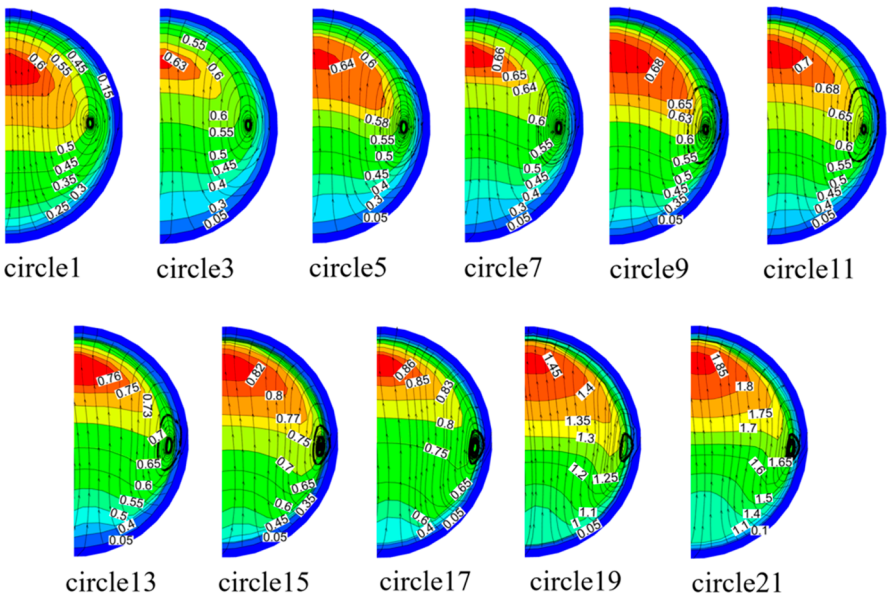

Figure 8. Cross-section velocity along the coiled tube.

error is up to 5%, including measurement and acquisition errors.

Numerical wall temperature distribution along the coiled tube is gradually increased in Figure 6. Figure 7 shows the half cross-section temperature along the coiled tube, and Figure 8 shows the cross-section velocity and streamlines. We define the axial direction facing the center as the inner wall and the other direction as the outer wall. As shown, the upward direction is the outer wall and the downward direction is the inner wall. The temperature contour of the cross-section is slightly changed in the core but changes fast near the wall, and the maximum temperature takes place near the inner side. Secondary flows lead to a pair of symmetrical vortices in the cross-section and the fluid trajectory is in the form of a double

https://doi.org/10.1021/acsomega.2c02848
ACS Omega 2022, 7, 23978−23987

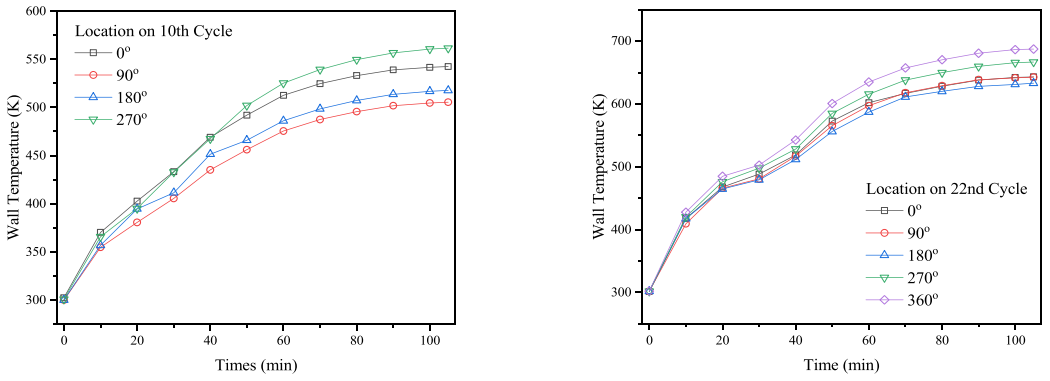

Figure 9. Variation of outer wall temperature with time (a, no. 10; b, no. 22).

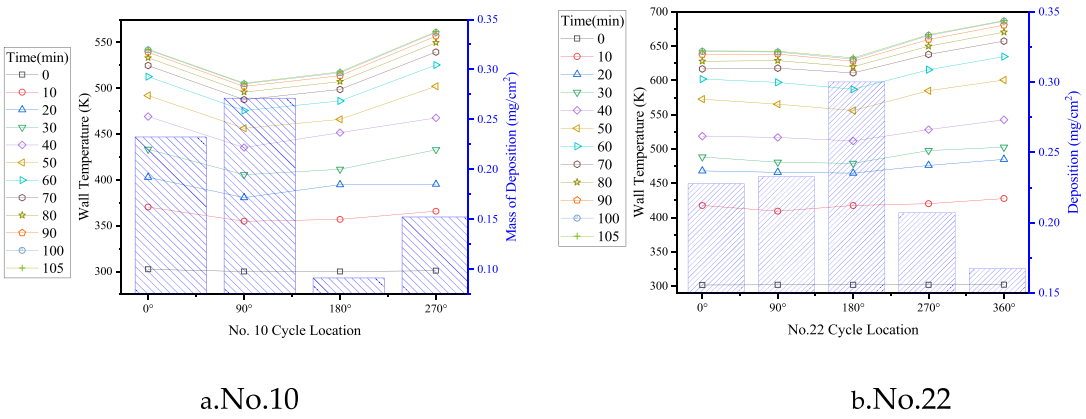

Figure 10. Wall temperature and deposition of each section of 10th and 22nd turns of the coiled tube (a, no. 10; b, no. 22).

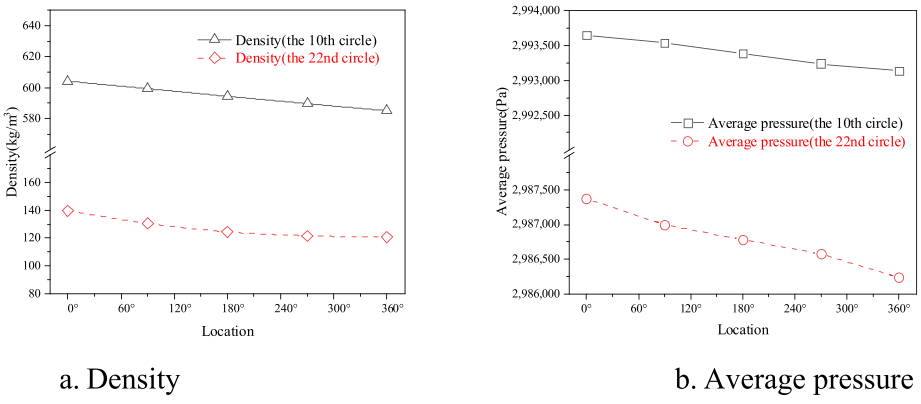

Figure 11. Density and average pressure of cross-section along 10th and 22nd turns of the coiled tube (a, density; b, average pressure).

coil. The unbalanced centrifugal forces of the main flow result in the shift of the maximum velocity fields to the outer wall. Because of the particular structure of the coiled, the fluid will generate centrifugal force during the flow process, and centrifugal force will cause secondary flow in the mainstream direction, that is, Dean Vortex. At the same time, buoyancy will be generated in the heating pipe, and buoyancy will also cause secondary flow, that is, the so-called Morton vortex. Secondary flows displace the position of the maximum total pressure toward the outside of the tube. The flow is fully developed along the coil, and secondary flows dominate the flow field. As the flow progresses, the structure of the secondary flow gradually becomes smaller. As the temperature rises above the critical temperature, the physical properties of the fluid change significantly, resulting in the increase of the flow velocity.

In order to further study the flow heat transfer and deposition characteristics of a single coil in the spiral tube heat exchanger, thermocouples were arranged outside the heat exchange tube at an interval of 90° along the 10th and 22nd coils of the heat exchanger as shown in Figure 2b, and the deposition results were measured, respectively. Figure 9 shows the wall temperature variation along the 10th and 22nd cycles with time. It can be seen that the temperature variation trend of each point is the same within the first 10 min. This is a process of the gradual establishment of the flow field, low fuel temperature, and relatively simple flow in the pipe. After 10

https://doi.org/10.1021/acsomega.2c02848
ACS Omega 2022, 7, 23978−23987

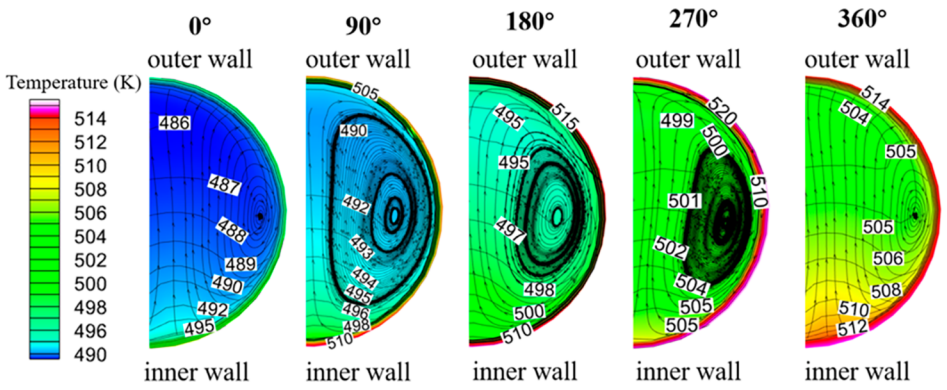

Figure 12. Cross-section temperature and velocity contours along the 10th circle.

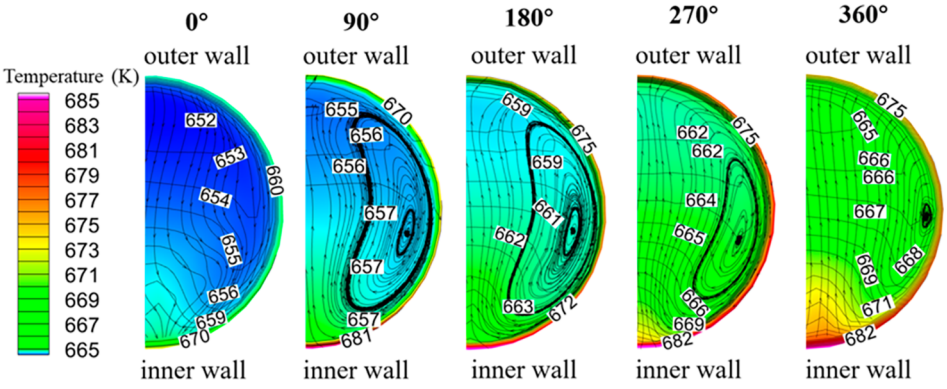

Figure 13. Cross-section temperature and velocity contours along the 22nd circle.

min, the changing trend of wall temperature at each point along the process begins to be different. After a period of rising, it gradually tends to a stable heat balance state. There is a nonlinear increase in the 22nd cycle, mainly because the fuel is already in the supercritical state and the Re number is also at a high level, resulting in the further complexity of the fuel flow development. In this way, the heat transfer is affected by the combined action of supercritical characteristics, secondary flow, and buoyancy. The results of temperature and deposition in the two circles are compared in Figure 10. By comparing the distribution of wall temperature in each section, the influence of flow on heat exchange after heating is more prominent. At the same time, it reveals that there would be a heat-exchange enhancement process from the temperature rising section to the falling section, which also brings changes in the deposition. There is a higher amount of deposition near the lower temperature due to the formation of a temperature gradient induced by enhanced heat transfer.[11] At the same time, the solubility of deposition precursors will be reduced and deposited in the low temperature area. Because the experimental time is 1.75 h, the total amount of deposition is relatively small, and the deposition has little effect on heat exchange. Generally, when the heating time is more than 2 h, there is an obvious obstruction to heat exchange. At the same time, due to the complex flow of spiral tube and the effect of secondary flow, the effect of deposition on heat exchange could not be classified independently in the coiled tube in this study. The results of density and average pressure in the two circles are compared in Figure 11. With the continuous inflow of heat flow, the fluid reaches the critical state and its density, viscosity, and other parameters are reduced, which enhances the effect of buoyancy and increases the flow speed. The strength of the centrifugal force on the cross-section decreases, and so does the strength of the secondary flow.

In order to further study the flow state in these two circles, Figure 12 and Figure 13 show the calculation results of the temperature distribution and velocity of the 10th and 22nd circle of the coiled tube, respectively. It can be found that the maximum temperature difference inside the two rings is about 40 K and the temperature on the inner wall is always higher than that on the outer wall. The temperature on each section is nonuniformity. With the increase of flow length, the temperature nonuniformity on the flow section increases gradually under the influence of centrifugal force. At the cross-section of the 22nd circle, the temperature exceeds the critical temperature of the fluid, which also leads to an increase in the nonuniformity of the flow and affects the temperature distribution. Considering the profiles in Figure 10 and the simulation results in Figures 12 and 13, the heat-transfer coefficient has a periodic distribution in the flow direction. The maximum value appears in the vertical rise (90°) and the descending section (270°) of the coiled tube. The temperature on both sides of the section is almost similar. The external temperature is obviously greater than the internal temperature, and the temperature distribution is symmetrical about the horizontal line from inside to outside. This shows that centrifugal force plays a dominant role compared with buoyancy force. Figure 14 shows contours of dimensionless total pressure $((P - p_0)/\frac{1}{2}\rho U_{max}^2)$ along the 10th circle,[39] which are of the difference between the total pressure (P) and the static pressure (P_0) at the start of the bend divided by the maximum velocity head $(\frac{1}{2}\rho U_{max}^2)$ of the first bend (0°). The secondary flow pushes the position of maximum total pressure

https://doi.org/10.1021/acsomega.2c02848
ACS Omega 2022, 7, 23978−23987

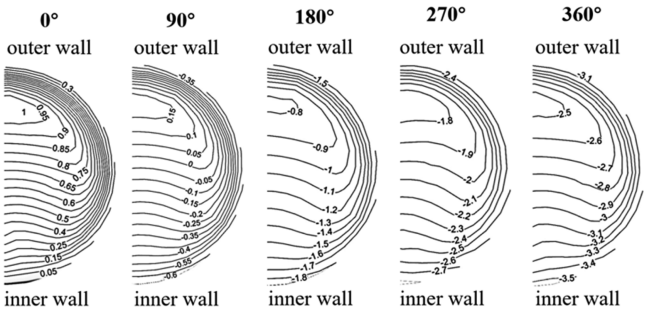

Figure 14. Contours of dimensionless total pressure along the 10th circle.

toward the outside of bends; thus, the contour lines can reflect the development state of secondary flow, and it can be seen that the secondary flow has entirely developed in the 10th circle and the pressure shows a trend of uniform decline in the flow direction.

The heat transfer has been investigated at different flow rates from 0.5 to 3 g/s and heat fluxes from 25 to 65 kW/m^2. The flow regime in the coiled tube is dominated by the secondary flow, which is affected by the Dean number, defined as $D_e = R_e\sqrt{\frac{r}{R}}$,[40] where R_e is the Reynolds number, r is the radius of the pipe, and R is the radius of curvature of the pipe axis.

Most of the previous research[22,23,32,41] on the Nu number of the coiled tube was conducted at low Reynolds number and low temperature, while there was also some research on aviation kerosene in the coiled tube at high Reynolds numbers and high temperatures. The heat-transfer correlation of the coiled tube can be based on a general correlation for forced convection heat transfer, that is, the Dittus−-Boelter correlation as $Nu_o = 0.0243Re_b^{0.8}pr_b^{0.4}$.[42] Supercritical properties of the fuel are taken into account by the function of the boundary layer. The Nusselt number correlation of the supercritical fuel in the coiled tube is modified as

$$\frac{Nu}{Nu_o} = 0.0741\left(\frac{\rho_f}{\rho_b}\right)^{0.2942}\left[1 + 21.4\left(\frac{d}{x}\right)\right](1 + De^{-0.7993})\left[1 + 11.75\left(\frac{Nu}{Nu_o}\right)^{1.102}\right] \quad (5)$$

where the exit effect is considered and corrected by the function of $\rho_f = \frac{\int_{T_b}^{T_w}\rho(T)\,dT}{T_w - T_b}$ in which d is the inner diameter of the tube and x is the position along fluid direction. In the subscript, f represents the supercritical properties of the boundary layer effect calculated as $\frac{d}{x}$, and b is a calculated value; w is the measured wall temperature. The comparison of the results calculated by the modified correlation equation and the experimental data is plotted in Figure 15. The error between the experimental and calculated values is within ±10%.

4. CONCLUSIONS

A coiled tube 3000 mm long and with 23 cycles has been employed as the heat exchanger to investigate the deposition and heat-transfer characteristics of supercritical aviation fuel RP-3 both in experimental and numerical methods. The flowing heating experiments show that the relatively high

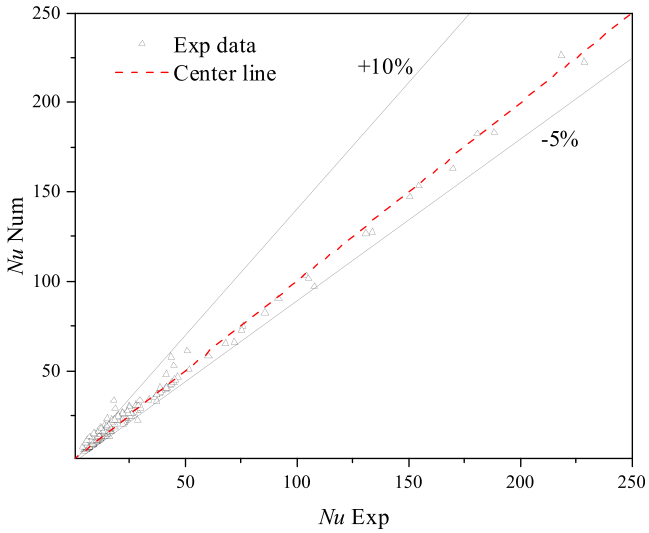

Figure 15. Comparison of the results calculated by the modified correlation equation and experimental data in the coiled tube.

Reynolds number and turbulent flow in the coiled tube considerably enhance heat transfer and decrease the deposition rates. Compared with straight tubes in the reference work, coiled tubes have a more uniform coking distribution and do not show obvious areas of coking deterioration. The effect of secondary flow and centrifugal force leads to the transformation of flow patterns in the spiral tube, which greatly influences pressure and temperature distribution in the spiral tube. Along the flow, the secondary flow structure decreases as the fluid gradually enters the supercritical state. The effects of secondary flows in the coiled tube are illustrated numerically in the distribution of dynamic pressure, temperature, and velocity in the circular cross-section located in the middle of the tube. The secondary flow development is almost complete in the front part of the coiled tube, which makes the dynamic pressure, pressure, and temperature change with the flow in a single trend. Finally, considering the effects of supercritical properties of the fuel, boundary layer, secondary flow, and exit effect, the correlation of heat transfer in the coiled tube is modified based on the experimental data of the aviation fuel of RP-3. The modified heat-transfer correlation of the supercritical RP-3 in the coiled tube has been fitted, and the error is within ±10%.

AUTHOR INFORMATION

Corresponding Authors

Xinyan Pei − *Institute for Aero Engine, Tsinghua University, Beijing 100084, China;* orcid.org/0000-0003-2407-9086; Email: peixinyan@mail.tsinghua.edu.cn

Lingyun Hou − *Institute for Aero Engine, Tsinghua University, Beijing 100084, China;* orcid.org/0000-0001-9013-9265; Email: lyhou@tsinghua.edu.cn

Authors

Hongyu Tian − *Institute for Aero Engine, Tsinghua University, Beijing 100084, China*

Zekun Zheng − *School of Aerospace Engineering, Tsinghua University, Beijing 100084, China*

Yafen Wang − *Institute for Aero Engine, Tsinghua University, Beijing 100084, China*

Complete contact information is available at:

https://doi.org/10.1021/acsomega.2c02848
ACS Omega 2022, 7, 23978−23987

https://pubs.acs.org/10.1021/acsomega.2c02848

Author Contributions

Xinyan Pei: Conceptualization, Writing-original draft, Investigation. Hongyu Tian: Writing, Data curation. Zekun Zheng: Writing, Review and Editing. Yafen Wang: Writing, Review and Editing. Lingyun Hou: Methodology, Supervision, Review and Editing.

Notes

The authors declare no competing financial interest.

■ ACKNOWLEDGMENTS

This work was financially supported by the National Natural Science Foundation of China (Grant No. 52006122) and Science and Technology on Scramjet Laboratory (Grant No. 2021-JCJQ-LB-020-06).

■ REFERENCES

(1) Bruening, G. B.; Chang, W. S. Cooled Cooling Air Systems for Turbine Thermal Management. *American Society of Mechanical Engineers* **1999**, DOI: 10.1115/99-GT-014.

(2) Tibbs, G. B. Test results of the Northrop Grumman Corporation Turbine Engine Bleed Air/Fuel Heat Exchanger after 165 h of operation with JP-8 + 100 fuel. *AIAA and SAE, 1998 World Aviation Conference (AIAA)* **1998**, DOI: 10.4271/985559.

(3) Nir, A., Three fluid heat exchanger. US 5893411A 1999.

(4) Nacke, R. A. *Air-to-fuel heat exchanger for high mach flow turbine engines*. M.S.M.E. Thesis, 2009.

(5) Nacke, R.; Northcutt, B.; Mudawar, I. Theory and experimental validation of cross-flow micro-channel heat exchanger module with reference to high Mach aircraft gas turbine engines. *International Journal of Heat & Mass Transfer* **2011**, *54* (5−6), 1224−1235.

(6) Holmes, J.; Lam, C.; Marx, B.; O'Brien, C. *Design and Demonstration of a Heat Exchanger for a Compact Natural Gas Compressor*; Worcester Polytechnic Institute, 2012.

(7) Manteufel, R. D.; Vecera, D. G. Consideration of Uncertainties in Compact Cross-Flow Heat Exchanger Design for Gas Turbine Engine Application; *ASME Turbo Expo 2013: Turbine Technical Conference and Exposition, American Society of Mechanical Engineers Digital Collection*, 2013.

(8) Kim, S.; Min, J. K.; Man, Y. H.; Son, C. Investigation of high-speed bypass effect on the performance of the surface air-oil heat exchanger for an aero engine. *International Journal of Heat & Mass Transfer* **2014**, *77* (oct), 321−334.

(9) Sundén, A.; Saidi, B. Bengt, Numerical simulation of turbulent convective heat transfer in square ribbed ducts. *Numerical Heat Transfer* **2000**, *38* (1), 67−88.

(10) Edwards, T.; Harrison, W.; Zabarnick, S.; Dewitt, M.; Bentz, C. Update on the Development of JP-8 + 100. *AIAA/ASME/SAE/ASEE Joint Propulsion Conference & Exhibit*, 2013.

(11) Pei, X. y.; Hou, L. y. Effect of dissolved oxygen concentration on coke deposition of kerosene. *Fuel Process. Technol.* **2016**, *142* (Supplement C), 86−91.

(12) Pei, X.; Hou, L., Experimental Study on the Layer Properties of RP-3 Oxidation Deposition. In *21st AIAA International Space Planes and Hypersonics Technologies Conference*; American Institute of Aeronautics and Astronautics, 2017.

(13) Spadaccini, L. J.; Sobel, D. R.; Huang, H. Deposit Formation and Mitigation in Aircraft Fuels. *Journal of Engineering for Gas Turbines & Power* **2001**, *123*, 741.

(14) Spadaccini, L. J.; He, H. On-Line Fuel Deoxygenation for Coke Suppression. *Journal of Engineering for Gas Turbines & Power* **2002**, *125* (3), 369−377.

(15) Morris, R. E.; Johnson, K. J.; Digiulio, C. *Examination of JP-8 Fuels for Contaminants Responsible for KC-130J. Nozzle Fouling*; NRL/MR/6180-06-8960; Naval Research Laboratory: Washington, DC, 2006; p 17.

(16) Evans, A., Jr.; Hibbard, R.; Watt, J. *Fouling characteristics of ASTM jet A fuel when heated to 700 deg F in a simulated heat exchanger tube*; Lewis Research Center, Cleveland, OH, 1968.

(17) Jones, E. G.; Balster, L. M.; Balster, W. J. Autoxidation of Aviation Fuels in Heated Tubes: Surface Effects. *Energy Fuels* **1996**, *10* (3), 831−836.

(18) Jiang, H.; Ervin, J.; West, Z.; Zabarnick, S. Turbulent Flow, Heat Transfer Deterioration, and Thermal Oxidation of Jet Fuel. *Journal of Thermophysics & Heat Transfer* **2013**, *27* (4), 668−678.

(19) Kuprowicz, N. J.; Zabarnick, S.; West, Z. J.; Ervin, J. S. Use of measured species class concentrations with chemical kinetic modeling for the prediction of autoxidation and deposition of jet fuels. *Energy Fuels* **2007**, *21* (2), 530−544.

(20) Tao, Z.; Fu, Y.; Xu, G.; Deng, H.; Jia, Z. Experimental study on influences of physical factors to supercritical RP-3 surface and liquid-space thermal oxidation coking. *Energy Fuels* **2014**, *28* (9), 6098−6106.

(21) Pei, X. Y.; Hou, L. Y.; Ren, Z. Y. Kinetic Modeling of Thermal Oxidation and Coking Deposition in Aviation Fuel. *Energy Fuels* **2017**, *31* (2), 1399−1405.

(22) Yildiz, C.; Bicer, Y.; Pehlivan, D. Heat transfers and pressure drops in rotating helical pipes. *Applied Energy* **1995**, *50* (1), 85−94.

(23) Rao, B. K. Turbulent heat transfer to power-law fluids in helical passages. *International Journal of Heat and Fluid Flow* **1994**, *15* (2), 142−148.

(24) Austen, D. S.; Soliman, H. M. Laminar flow and heat transfer in helically coiled tubes with substantial pitch. *Experimental Thermal and Fluid Science* **1988**, *1* (2), 183−194.

(25) Chingulpitak, S.; Wongwises, S. Effects of coil diameter and pitch on the flow characteristics of alternative refrigerants flowing through adiabatic helical capillary tubes. *International Communications in Heat & Mass Transfer* **2010**, *37* (9), 1305−1311.

(26) Ferng, Y. M.; Lin, W. C.; Chieng, C. C. Numerically investigated effects of different Dean number and pitch size on flow and heat transfer characteristics in a helically coil-tube heat exchanger. *Applied Thermal Engineering* **2012**, *36* (none), 378−385.

(27) Zhang, W.; Wang, S.; Li, C.; Xu, J. Mixed convective heat transfer of CO2 at supercritical pressures flowing upward through a vertical helically coiled tube. *Applied Thermal Engineering* **2015**, *88*, 61−70.

(28) Wang, K.; Xu, X.; Wu, Y.; Liu, C.; Dang, C. Numerical investigation on heat transfer of supercritical CO2 in heated helically coiled tubes. *J. Supercrit. Fluids* **2015**, *99*, 112−120.

(29) Lin, C. X.; Ebadian, M. A. Developing turbulent convective heat transfer in helical pipes. *International Journal of Heat & Mass Transfer* **1997**, *40* (16), 3861−3873.

(30) Lin, C. X.; Ebadian, M. A. The effects of inlet turbulence on the development of fluid flow and heat transfer in a helically coiled pipe. *International Journal of Heat & Mass Transfer* **1999**, *42* (4), 739−751.

(31) Pioro, I. L.; Duffey, R. B. Experimental heat transfer in supercritical water flowing inside channels (survey). *Nucl. Eng. Des.* **2005**, *235* (22), 2407−2430.

(32) Wang, K. Z.; Xu, X. X.; Liu, C.; Bai, W. J.; Dang, C. B. Experimental and numerical investigation on heat transfer characteristics of supercritical CO2 in the cooled helically coiled tube. *Int. J. Heat Mass Transfer* **2017**, *108*, 1645−1655.

(33) Pei, X.; Hou, L.; Mo, C.; Dong, N. Thermo-physical Properties for Surrogate Models of Aviation Kerosene. *J. Aerospace Power* **2015**, *30* (9), 2122−2128.

(34) Pei, X. Y.; Hou, L. Y.; Ren, Z. Y. Flow Pattern Effects on the Oxidation Deposition Rate of Aviation Kerosene. *Energy Fuels* **2015**, *29* (9), 6088−6094.

(35) Ansys, A. F. 14.0 Theory Guide. *ANSYS inc* **2011**, 390−391.

(36) Pei, X. Y.; Hou, L. Y. Effect of different species on physical properties for the surrogate of aviation fuel. *Journal of tsinghua university(science and technology)* **2017**, *7* (57), 774−780.

(37) Zhu, K.; Tao, Z.; Xu, G.; Jia, Z. Surface deposition characteristics of supercritical kerosene RP-3 fuel within treated and

untreated stain steel tubes: Part I Short thermal duration. *Energy Fuels* **2016**, *30* (4), 2687−2693.
(38) Liu, Z.; ang, S. T.; Li, Z.; Qin, Z.; Yuan, S.; Wang, L.; Wang, L.; Zhang, X.; Liu, G. An improved kinetic model for deposition by thermal oxidation of aviation hydrocarbon fuels. *Fuel* **2019**, *258* (Dec 15), 116139.1−116139.12.
(39) Rowe, M. Measurements and computations of flow in pipe bends. *J. Fluid Mech.* **1970**, *43* (4), 771−783.
(40) Mori, Y.; Nakayama, W. Study on forced convective heat transfer in curved pipes. *Int. J. Heat Mass Transfer* **1967**, *10* (5), 681−695.
(41) Fu, Y.; Wen, J.; Zhang, C. An experimental investigation on heat transfer enhancement of sprayed wire-mesh heat exchangers. *Int. J. Heat Mass Transfer* **2017**, *112*, 699−708.
(42) Winterton, R. Where did the Dittus and Boelter equation come from? *International Journal of Heat & Mass Transfer* **1998**, *41* (4-5), 809−810.

https://doi.org/10.1021/acsomega.2c02848
ACS Omega 2022, 7, 23978−23987